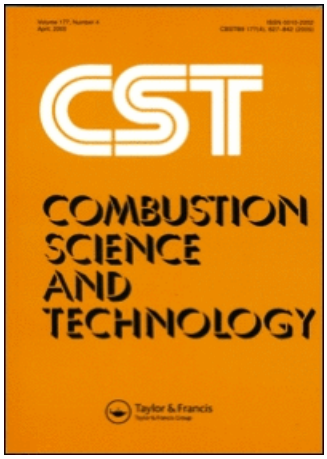

Combustion Science and Technology
Publication details, including instructions for authors and subscription information:
http://www.informaworld.com/smpp/title~content=t713456315

SMOLDERING COMBUSTION OF "INCENSE" STICKS - EXPERIMENTS AND MODELING

H. S. Mukunda [a]; J. Basani [a]; H. M. Shravan [a]; Binoy Philip [a]
[a] Department of Aerospace Engineering, Indian Institute of Science, Bangalore, India

Online Publication Date: 01 June 2007
To cite this Article: Mukunda, H. S., Basani, J., Shravan, H. M. and Philip, Binoy (2007) 'SMOLDERING COMBUSTION OF "INCENSE" STICKS - EXPERIMENTS AND MODELING', Combustion Science and Technology, 179:6, 1113 - 1129
To link to this article: DOI: 10.1080/00102200600970019
URL: http://dx.doi.org/10.1080/00102200600970019

Combust. Sci. and Tech., 179: 1113–1129, 2007

ISSN: 0010-2202 print/1563-521X online
DOI: 10.1080/00102200600910019

Smoldering Combustion of "Incense" Sticks—Experiments and Modeling

H. S. Mukunda,* J. Basani, H. M. Shravan, and Binoy Philip
Department of Aerospace Engineering, Indian Institute of Science, Bangalore, India

Abstract: This paper is concerned with the experimental and modeling studies on the smoldering rates of incense sticks as a function of ambient oxygen fraction in air, the flow velocity and size. The experimental results are obtained both for forward and reverse smolder conditions. The results are explained on the basis of surface combustion due to diffusion of oxygen to the surface by both free and forced convection supporting the heat transfer into the solid by conduction, into the stream by convection and the radiant heat transfer from the surface. The heat release at the surface is controlled by the convective transport of the oxidizer to the surface. To obtain the diffusion rates particularly for the reverse smolder, CFD calculations of fluid flow with along with a passive scalar are needed; these calculations have been made both for forward and reverse smolder. The interesting aspect of the CFD calculations is that while the Nusselt umber for forward smolder shows a clear $\sqrt{\mathrm{Re}_u}$ dependence (Re_u = Flow Reynolds Number), the result for reverse smolder shows a peak in the variation with Reynolds number with the values lower than for forward smolder and unsteadiness in the flow beyond a certain flow rate. The results of flow behavior and Nusselt number are used in a simple model for the heat transfer at the smoldering surface to obtain the dependence of the smoldering rate on the diameter of the incense stick, the flow rate of air and the oxygen fraction. The results are presented in terms of a correlation for the non-dimensional smoldering rate with radiant flux from the surface and heat generation rate at the surface. The correlations appear reasonable for both forward and reverse smolder cases.

Keywords: Convection; Gasification; Incense sticks; Nonporous charring fuel; Smoldering combustion

Received 21 February 2003; accepted 19 July 2006.
*Address correspondence to mukunda@cgpl.iisc.ernet.in

INTRODUCTION

Smoldering combustion is extensively studied in literature (a review is available in Ohlemiller, 1985, 1995). Nearly all this literature is concerned with smoldering combustion through porous media essentially emanating from fire related problems. Blasi (1993), Kashiwagi (1994) and Kashiwagi and Ohlemiller (1982) have examined the condensed phase processes with polymers such as polymethylmethacrylate and polyethylene including the role of oxygen in the gas phase on the gasification. Esfahani (2002) has proposed a model for the thermal behavior in an oxidative environment for non-charring polymers such as PMMA. Calculations are made for the in-depth thermal profile with impinging heat flux from thermal radiation and these are shown to be in reasonable agreement with measurements of Kashiwagi (1994) and others. Olsen and T'ien (2000) have experimentally studied the flame structure and extinction characteristics of a buoyancy induced diffusion flame beneath a cylindrical PMMA sample. The study reveals that the fraction of heat transfer from the flame lost to in-depth conduction and surface radiation increases towards quenching conditions. This is argued to be due to decreased heat transfer from the flame with the losses remaining unaltered.

The present problem involving smoldering of a nonporous charring solid (both in forward and reverse smolder modes) is not covered by the above studies. There is a passing reference by Williams (1976) in his discussion on the mechanisms of fire spread. Incense sticks are used on many occasions to spread a pleasant aroma from the chemicals released during the process of gasification. The incense sticks can also be burnt under flaming conditions. In the case of flaming combustion, the combustion is gas phase dominated and in the case of smoldering combustion, it is heterogeneous reaction dominated. The solid-to-gas conversion occurs much faster in flaming combustion than in smoldering combustion. The latter mode of conversion is considered in the present study. Beyond a level of oxygen fraction in the oxidant stream, the conversion process in a collection of a large number of incense sticks transitions to flaming. The flaming regime is not a subject of discussion here, since most often, when they are used, incense sticks are not subject to such conditions.

EXPERIMENTS

Figure 1 shows the experimental set up. A sample holder is fixed in a duct 40 mm dia., 250 mm long. This circular glass tube segment through which air/enriched air is passed is preceded by a 63 mm dia., 400 mm long and a mixing chamber 126 mm dia. and 500 mm long. A blower delivers air into the mixing chamber. The desired amount of oxygen is injected into the

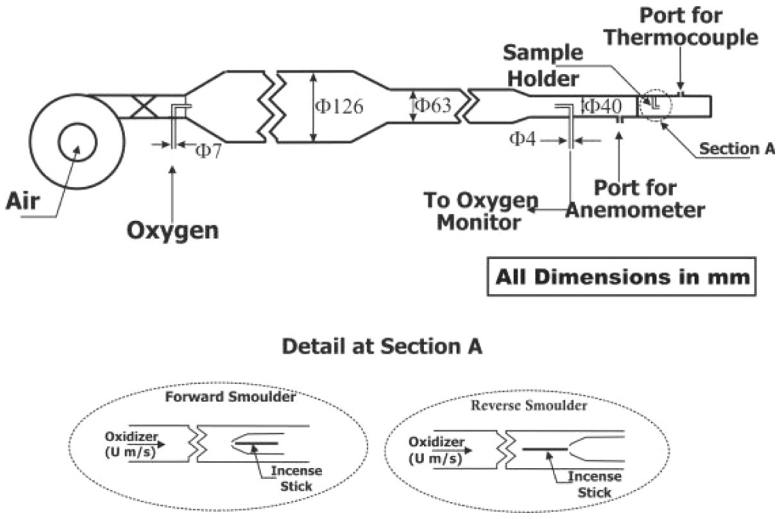

Figure 1. The experimental setup.

mixing chamber from a high-pressure oxygen cylinder. The long line available for the fluid flow is expected to cause mixing of the streams into a homogeneous composition. Of course, this is established by a measurement of the composition across the cross section in the sample holder area. An arrangement of incense sticks, which may consist of one or more of these bunched together, is fixed to a sample holder in the same direction as that of the flow around it or opposing the airflow.

The oxygen fraction in the fluid stream is measured close to the sample holder with a non-dispersive oxygen analyzer through which a small amount of fluid is drawn with a pump. Stream velocity is measured using a hot wire anemometer across the section close to the central zone where the sample holder is kept. A check on the relative flow rates was made periodically using a calibrated venturi to measure the total flow through the system. Smoldering rates were measured by timing the regression for different segments marked on the incense stick. Measurement of the surface temperature was attempted in select experiments by using a 50 μm (Pt − Pt + 13% Rh) thermocouple whose bead about 100 μm dia. was drawn against the hot front end of the burning incense stick.

The incense sticks that were used in the experiments were procured from commercial sources. These are produced in an industrial sector, the typical composition being 90–95% sawdust, 4–9% powdered charcoal, 0.1–1% of an aroma producing chemical and the rest, a biomass binder to enable rolling of the soft mass around a support wood stick. The incense sticks so produced are then dried and packed. The core diameter of the support stick varied from 0.3 mm to 0.6 mm. Incense stick

smoldering with larger support stick diameter showed a conical smolder front. Even though there were no significant differences in the smolder rates between the two types, most experiments were restricted to small support diameter sticks to reduce the influence of support stick. The density and ash content of the sticks were measured as 900 ± 50 kg/m^3 and 6.5–7%, respectively.

Experiments were conducted with single sticks (3 mm dia.), a bunch of three (5 mm dia.), five sticks (7 mm dia.) and 10 sticks (10 mm dia.). When more than one stick had to be used, the sticks were put together and covered by a cellophane tape throughout and at the ends as well so that there is no flow through the spaces between the sticks and one can assume that the bunch acts a stick of larger diameter. The stream velocity was varied from 0 to 7 m/s (but in most cases up to 4 m/s) and oxidizer fraction from 21–40% (by volume). When the stream velocity is zero, the smoldering process is controlled by free convection. Some experiments were repeated to determine the possible dispersion in the overall results to differences in the composition of the incense sticks. The results on smoldering rates are correct to $\pm$ 5%; stream oxygen fraction was controlled to within 5%. The surface temperatures are accurate to about $\pm$30 K.

When experiments were conducted without forced convection, ash was found to deposit at the end of the stick for long duration. This ash was periodically broken in a few experiments. The smoldering rate with and without ash build up did not show any specific trend. The smolder rates were within the differences due to other factors, primarily the production quality of the sticks themselves. It is inferred that the resistance of the porous ash layer would not be rate limiting at these smolder rates. In the case of forward smolder, the ash build up was taken away by the stream on a continuous basis. In the case of reverse smolder, the ash build up would crack up periodically and taken away by the stream.

EXPERIMENTAL RESULTS

Figure 2 shows the data on the smoldering rate with air velocity for forward smoldering as a function of diameter and oxygen fraction. As can be expected, the smoldering rate decreases with the size of the stick, and increases with the speed of the air stream. The stick size seems to have diminishing effect with air speed. Smolder rate increases with oxygen fraction. The experiments were limited to 40% since beyond this value, the smoldering process gave way to flaming combustion. The results for reverse smoldering for 3 mm stick diameter with oxygen fraction are presented in Figure 3. Here again, the results of increased smoldering rate with oxygen fraction are similar to that of forward smoldering; the peaking and further decrease of smoldering rate with

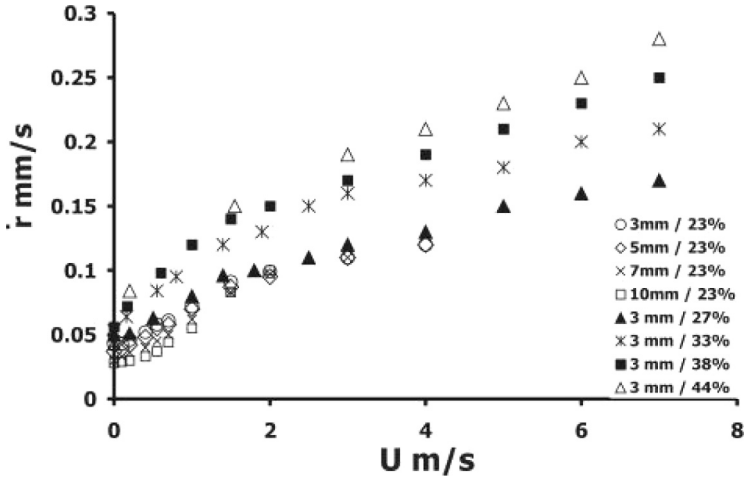

Figure 2. Experimental data on the forward smolder rate vs. stick diameter and oxygen fraction with stream velocity.

air velocity must be related to adverse heat balance due to reduced transport rate of oxygen to the surface.

The data on surface temperatures is plotted on $\dot{r}$ vs. $1000/T_s$ in Figure 4 expecting the relationship $\dot{r} = A_f \exp[-E/RT_s]$ where A_f the pre-exponential factor is, and E/R is the activation temperature and T_s is the surface temperature. These data translate into an expression $\dot{r}(\mathrm{m/s}) = 0.00382 \exp[-3500/\mathrm{T_s}]$. This is the pyrolysis rate expression for

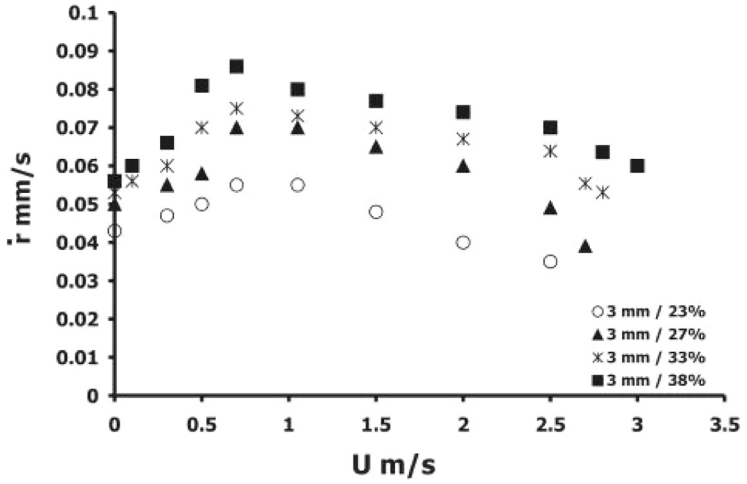

Figure 3. Reverse smoldering propagation at different oxygen fractions.

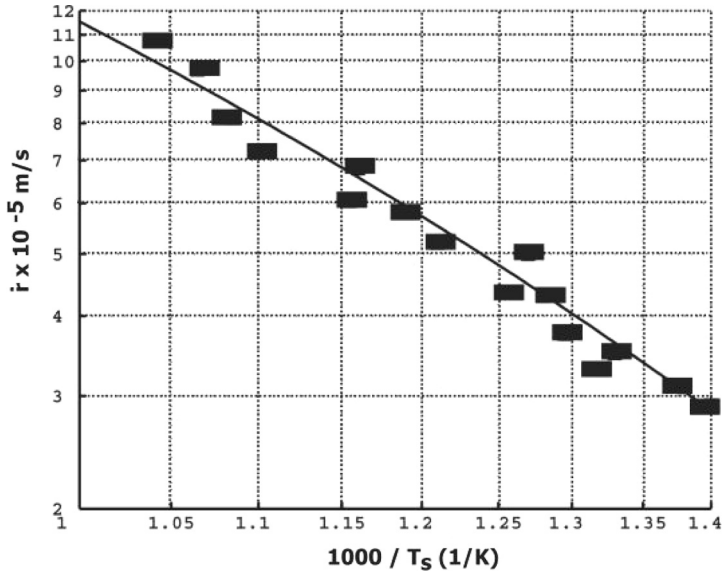

Figure 4. The plot of $\dot{r}$ vs $1000/T_s$.

the surface regression. As a part of the theory being developed, it was necessary to determine the heat of surface combustion. Towards this, the composition of the gas coming out of the surface was determined. A large number of sticks (about 30) were bundled together and were ignited and set into smoldering mode. The gas emanating from the sticks was sampled and analyzed for CO, CO_2, H_2, and CH_4 in a combined non-dispersive infrared analyzer. This showed the analysis to be CO = 4.0–4.5%, CO_2 = 16.5–17%, H_2 and CH_4, nearly zero and rest composed of nitrogen and water vapor.

THE MODEL

Figures 5a and 5b schematically show the processes modeled for forward and reverse smolder phenomena respectively. The model treats an ash free smoldering process based on the observations described earlier. Oxidizer transport to the ignited surface will lead to some diffusion through a thin layer wherein the reactions occur leading to heat release. This heat is largely conducted into the solid inside and some transferred to the stream by convection and radiation. The steady heat balance is written as (Heat release rate by surface reaction = Heat conduction into the solid + Heat transport into the stream + Radiant Heat loss to the ambient). This is expressed mathematically by

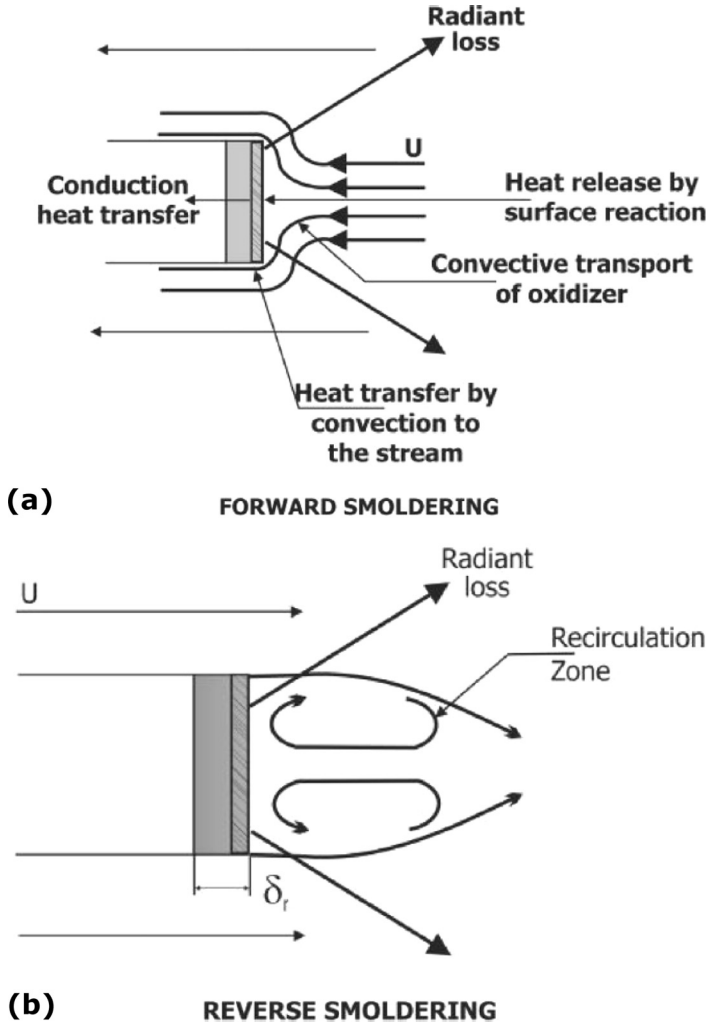

Figure 5. The schematic of heat and mass transfer in the reaction zone for forward and reverse smolder.

$$k\left[\frac{dT}{dy}\right]_{-} - k\left[\frac{dT}{dy}\right]_{+} + \varepsilon\sigma\left(T_s^4 - T_0^4\right) = HD\rho\left[\frac{dY_{ox}}{dy}\right]_{+} \tag{1}$$

In the preceding equation, the first term represents the conductive flux into the solid (region denoted by the subscript $-$), the second term represents the conductive flux into the gas phase and third term the radiant heat loss. The symbols are as follows: k is thermal conductivity, y is

the coordinate normal to the smoldering surface positive into the gas phase, subscripts − and + denote the zones in the condensed phase and the gas phase at the interface, [epsilon] and σ, the emissivity of the surface and the radiation constant (5.76×10^{-8} W/m^2 K^4), H is the heat of reaction of the surface with the oxygen transported to the surface, Y_{ox} is the oxygen mass fraction, D is the diffusion coefficient and ρ is the gas density. In this analysis, the heat release per unit mass of the incense stick (fuel), H is taken as constant (independent of the oxygen fraction in the stream). Enhanced free stream oxygen fraction alters the flux and hence the regression rate.

The conduction equation in the condensed phase can be written as

$$\rho_p \dot{r} c_p \frac{dT}{dy} = k \frac{d^2T}{dy^2} \tag{2}$$

where ρ_p is the density of the solid, c_p is the specific heat and $\dot{r}$, the smoldering rate. If we solve the equation with the conditions $T = T_s$ at $y = 0$ and $T = T_0$ as $y \to -\infty$ we obtain the gradient at $y = 0^-$ as

$$k\left[\frac{dT}{dy}\right]_- = \rho_p \dot{r} c_p (T_s - T_0) \tag{3}$$

We consider the gas phase now. The gas phase temperature gradient can be expressed as

$$k\left[\frac{dT}{dy}\right]_+ = h_y (T_s - T_0) = Nu \frac{k}{d_0} (T_s - T_0) \tag{4}$$

where h_g is the gas phase heat transfer coefficient, d_0 is the incense stick diameter and Nu, the Nusselt number. By expressing in this manner we can relate the heat transfer process in classical terms.

We take the Lewis number ($D\rho c_p/k$) and Schmidt number ($\mu/D\rho$) as unity. The first choice leads to the similarity between heat and mass transfer. This gives the equivalence of the flux terms as

$$D\rho \frac{[dY_{ox}/dy]_+}{Y_{ox,\infty}} = \frac{k}{c_p} \frac{[dT/dy]_+}{(T_s - T_0)} \tag{5}$$

where $Y_{ox,\infty}$ is the oxidant mass fraction in the free stream. By combining the above terms, we can express equation (1) as

$$\rho_p \dot{r} c_p (T_s - T_0) + \varepsilon\sigma (T_s^4 - T_0^4) = (B - 1) Nu \frac{k}{d_0} (T_s - T_0) \tag{6}$$

Where $B = HY_{ox,\infty}/c_p(T_s - T_0)$ is the transfer number for surface heat release. By defining $Re_r = \rho_p \dot{r} d_0/\mu$, $\mathrm{Re}_r = \rho_p \dot{r} d_0/\mu$ where Re_r is the smoldering Reynolds number, μ is the viscosity and invoking flow Reynolds

number (Re_u) and Grashof number (Gr) as $\mathrm{Re}_u = \rho U d_0/\mu$ and $Gr = [(T_s - T_0)/T_0]gd_0^3/[\mu/\rho]^2$, we can restate the above equation as

$$\mathrm{Re}_r + \frac{\varepsilon\sigma(T_s^4 - T_0^4)}{[\mu c_p/d_0](T_s - T_0)} = (B-1)Nu[\mathrm{Re}_u, Gr] \tag{7}$$

Since the observed smolder rate varies by a factor of more than four over the flow velocity range, one can expect that blocking effects are significant and need to be accounted. This is expressed by rewriting the above equation as

$$\mathrm{Re}_r + \frac{\varepsilon\sigma(T_s^4 - T_0^4)}{[\mu c_p/d_0](T_s - T_0)} = (B-1)\frac{Nu}{Nu_0}Nu_0[\mathrm{Re}_u, Gr] \tag{8}$$

The ratio Nu/Nu_0 that constitutes the blocking effect is known to be a function of transfer number, B. Studies by Kutataladze and Leontev (1964) and further examination by Paul et al. (1982) have shown that the blocking effect depends the density of gases being injected from the wall. This consists of polymeric material fragments, carbon dioxide and nitrogen that have an average molecular weight in the range of a few hundred. Hence the blocking effect is extracted from experimental data obtained from earlier work and presented in Paul et al (1982). In the range of transfer numbers of interest to this work, namely, 3–8, the quantity, can be represented by $0.7B^{0.75}$. The parameter that we need to obtain further is the Nusselt number (Nu_0) as a function of Reynolds and Grashof numbers for both forward and reverse smolder. One can expect the combined influence of free and forced convection to be present for a range of stream velocities $\sim\sqrt{gd_0}$ to about 0.16 to 0.3 m/s for the diameter range of 3 to 10 mm. For velocities much larger than this value one can expect the forced convection to dominate (the maximum velocity for most experiments was 4 m/s). In order to determine the Nusselt number one can use the correlations for both free and forced convection and combine them suitably. It is to be recognized that the range of Re_u for which experiments have been carried out is 0 to 2500, and the range for Grashof number is 1500 to 3000. In this range that is largely laminar (and only in some parts transitional), one can use the correlations (see Isachenko et al, 1977) as follows.

$$Nu_0 = 0.3\mathrm{Re}^{0.5} \tag{9}$$

$$Nu_0 = 0.70Gr^{0.25} \tag{10}$$

In the case of reverse smolder, it is not possible to use any correlations since the recirculating flow leads to velocities that are not easy to estimate. An examination of literature showed that the issue of heat transfer to the back wall had not been addressed, perhaps, because it is

not practically relevant except for the situation noted before. This necessitated the use of CFD tools to determine the mean heat transfer to the back wall. In order to assure that the computational procedure is calibrated, it was decided to compute the case of forward smolder and ensure that the results are consistent with known data and then the reverse smolder was examined.

TWO-DIMENSIONAL FLOW AND HEAT TRANSFER CALCULATIONS

The computations were performed on the 3 mm stick treating the smoldering surface as fixed by solving the conservation equations for flow and heat transfer with a fixed wall temperature of 800 K and a free stream temperature of 300 K with stream velocities from 0.01 to 3 m/s for both forward and reverse smolder. Commercially available software CFX TASCflow version 2.12.01 was used in the calculations including the option for free convection. Constant property assumption was used in making the calculations. The computational domain used and the boundary conditions imposed are presented in Figure 6. The code used a scheme that is second order accurate in space and first order accurate in time. The grid distribution was made such that the wall region had a

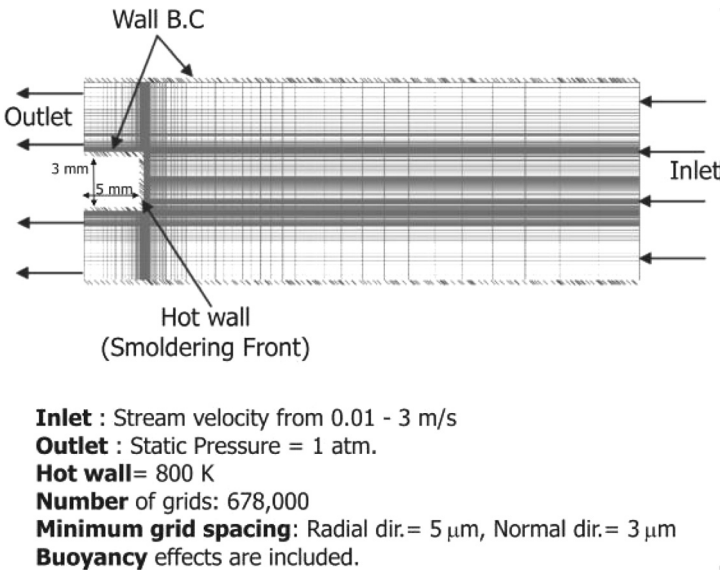

Figure 6. The computational domain and boundary conditions for forward and reverse smolder.

larger number of fine grids. The grid distribution was made finer with increasing stream speed. For the case of 3 m/s (forward smolder), the total number of grids used was 100,000 in the direction normal to the surface and 50,000 in the radial direction. The minimum grid spacing near the smoldering surface was 0.03 mm in the direction normal to the surface and 0.05 mm in the radial direction. Typical cell Reynolds numbers are 3 and 5 for the above case. The independence of the solution with the number of grids was established before the results were accepted. Steady solution was featured by the reduction in residuals of more than five orders of magnitude in all cases of forward smolder and for cases where the velocity was equal to and less than 1 m/s for reverse smolder. In cases of reverse smolder at stream speeds of 2 and 3 m/s the flow did not reach steady state, but an oscillatory reverse flow region was observed. The calculations were carried out for a sufficiently long flow time to cover the complete cycle of the oscillatory flow.

Figure 7 shows the wall temperature vs. normal distance for the case of 1 m/s for forward and reverse smolder for which steady solutions were obtained. The enhanced thermal boundary layer thickness for the case of reverse smolder is evident. Figure 8 shows the velocity vector plot for the case of reverse smolder for 2 m/s at four moments including those at which peak and low wall heat flux is received. One can observe the flow asymmetry caused because of buoyancy due to the hot wall. The recirculation zone is about 1.5 to 1.7 times the stick diameter (or back-wall height). Typical reverse flow velocities are about 50–70% of the stream

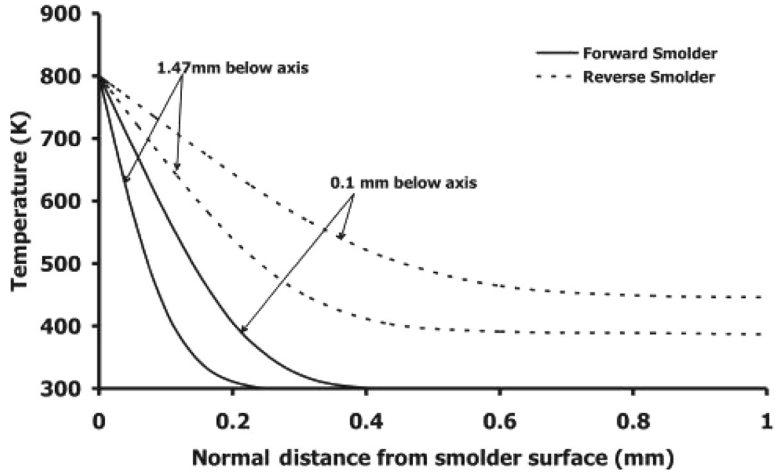

Figure 7. The temperature distribution normal to smoldering surface for 1 m/s case for forward and reverse smolder.

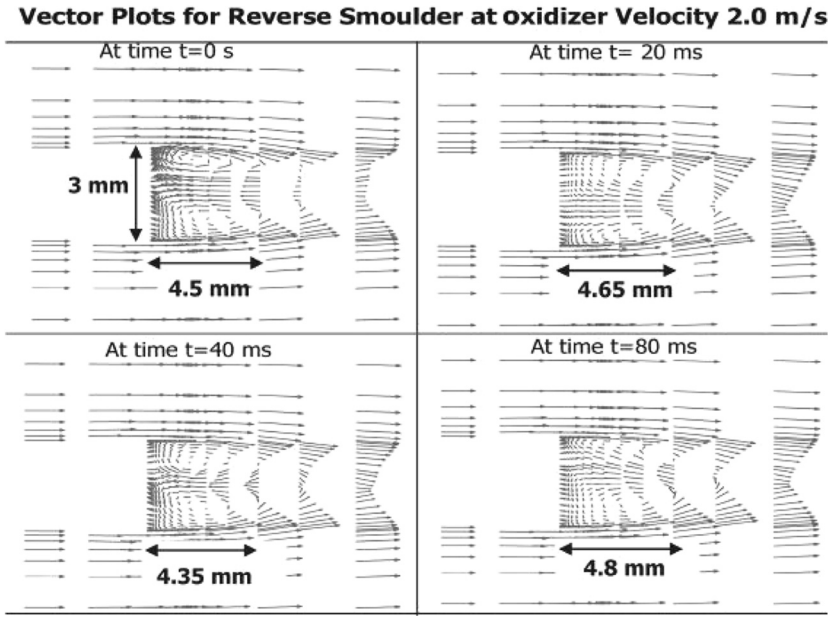

Figure 8. Velocity vector plot for the case of reverse smolder at a stream speed of 2 m/s.

speed. This contributes to the increase in boundary layer thickness next to the back wall and hence reduced heat transfer compared to forward smolder case.

The results from the calculations were processed as follows: First, the wall flux was obtained from the temperature gradients as a function of radial distance and an area weighted averaging technique was used to obtain a mean heat flux for each case. These were suitably non-dimensionalized (see Eq. (4)) to obtain the Nusselt number. The solutions obtained for cold flow showed skin friction coefficient vs. Re_u consistent with the results for laminar flow solutions with typical $\mathrm{Re}_u^{0.5}$ dependence. Figure 9 shows the plot of Nusselt number as a function of flow Reynolds number for both forward and reverse smolder configurations with wall maintained at 800 K to determine the behavior with free convective effects. The region bound by the two curves for the case of reverse smolder correspond to oscillatory flow behavior.

Figure 10 shows the Nusselt number as a function of flow time for a full cycle of the unsteady flow for 2 m/s case. It can be seen that the flow behavior is highly non-linear. Tracking this unsteady behavior called for fine time steps and fine space grid structure particularly near the wall. A curve fit of the Nu_0 vs. Re_u for forward smolder gives $Nu = 1.75\,\mathrm{Re}_u^{0.5}$.

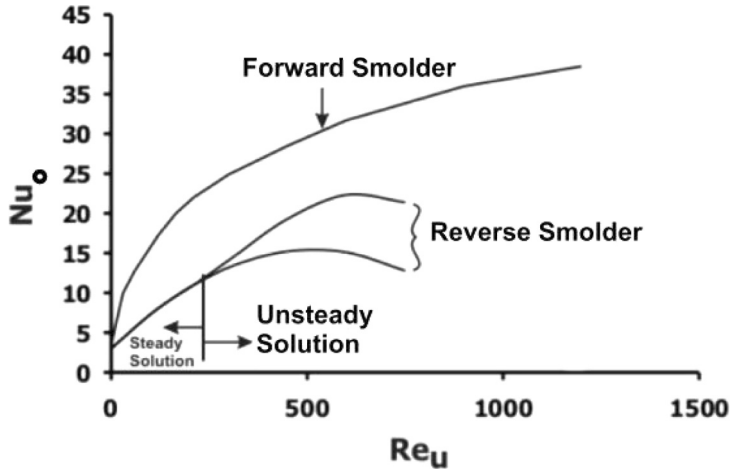

Figure 9. Nusselt number as a function of flow Reynolds number for forward and reverse smolder. Notice the upper and lower curves for reverse smolder that correspond to oscillatory flow behavior.

The difference between this result and that of Eq. (9) is due to the fact that the flux contribution in the outer radial regions of the stick is influenced by the flow turning process. Consequently, the choice of the constant is different from the classical value. For the case of reverse smolder, the behavior of Nu_0 with Re_u was used in the correlations.

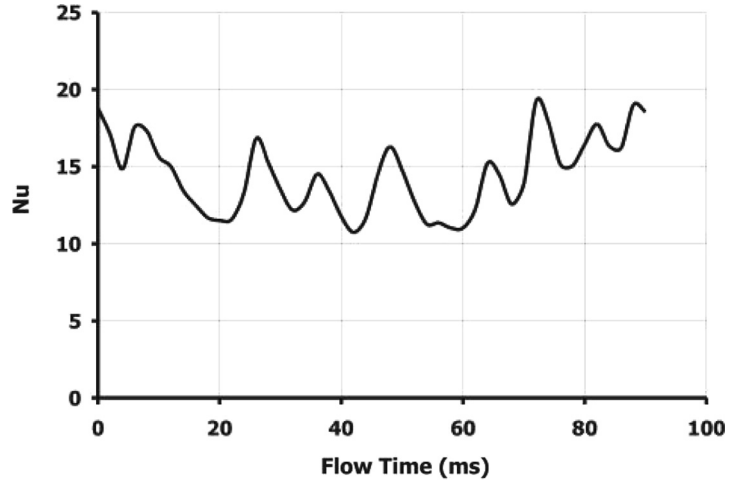

Figure 10. Nusselt number as a function of flow time for the case of reverse smolder at 2 m/s.

THE CORRELATIONS

Taking note of the variation of the Nusselt number with Grashof and Reynolds numbers, the expression for smolder rate given in Eq. (8) is cast as

$$\left[\mathrm{Re}_r + \frac{\varepsilon\sigma(T_s^4 - T_0^4)}{[\mu c_p/d_0](T_s - T_0)}\right] = 0.7B^{-0.75}[C_1 Gr^{0.25} + C_2 \mathrm{Re}_u^{0.5}] \qquad (11)$$

Equation (11) presents the results in terms of dimensionless flux balance. The left hand side can be interpreted as the heat flux absorbed by the condensed phase and the right hand side as the heat flux from the gas phase by combined free and forced convection. The constants C_1 and C_2 are to be determined from certain limiting conditions based on the cearlier discussion.

In order to facilitate comparison with experiments, Eq. (11) is expressed as

$$\left[\mathrm{Re}_r + \frac{\varepsilon\sigma(T_s^4 - T_0^4)}{[\mu c_p/d_0](T_s - T_0)}\right] \Big/ [0.7C_1 B^{0.75} Gr^{0.25}] = \left[1 + \frac{C_2}{C_1}\frac{\mathrm{Re}_u^{0.5}}{Gr^{0.25}}\right] \qquad (12)$$

Equation (11) can also be recast to express the dimensionless smolder rate in terms of other parameters.

$$\mathrm{Re}_r = 0.7B^{0.75}[C_1 Gr^{0.25} + C_2\ \mathrm{Re}_u^{0.5}] - \frac{\varepsilon\sigma(T_s^4 - T_0^4)}{[\mu c_p/d_0](T_s - T_0)} \qquad (13)$$

In order to check these relations against the data, various parameters are chosen as follows. $\rho_p = 900\,\mathrm{kg/m^3}$, $\mu = 1.2 \times 10^{-5}\,\mathrm{kg/ms}$, $c_p = 1000$ J/kgK, $H = 10$ MJ/kg, $T_0 = 300\,\mathrm{K}$, $T_s =$ from smolder rate data of experiments and the pyrolysis rate expression. Among these data, the data on H needs justification. Full heat release from the combustion of the stick leads to the release of energy of 15 MJ/kg. In the oxidative pyrolysis that takes place at the surface, combustible gases are generated. These can further burn in the gas phase with oxygen of the atmosphere. An estimate of the heat release was made with data on the composition of the gases from the smoldering surface and this resulted in the value for $H = 10 \pm 0.5\,\mathrm{MJ/kg}$. For the experimental data described in Figures 2 and 3, the above terms are calculated. Based on Eq. (10) and numerical studies on forced convection, $C_1 = C_2 = 0.7$. The expression on the left hand side (*LHS*) defined by

$$LHS = \left[\mathrm{Re}_r + \frac{\varepsilon\sigma(T_s^4 - T_0^4)}{[\mu c_p/d_0](T_s - T_0)}\right] \Big/ [0.49B^{0.75} Gr^{0.25}] \qquad (14)$$

is plotted against $\mathrm{Re}_u^{0.5}/Gr^{0.25}$ in Figure 11. It can be seen that most the data fits into a band of the predictions to within $\pm 10\%$.

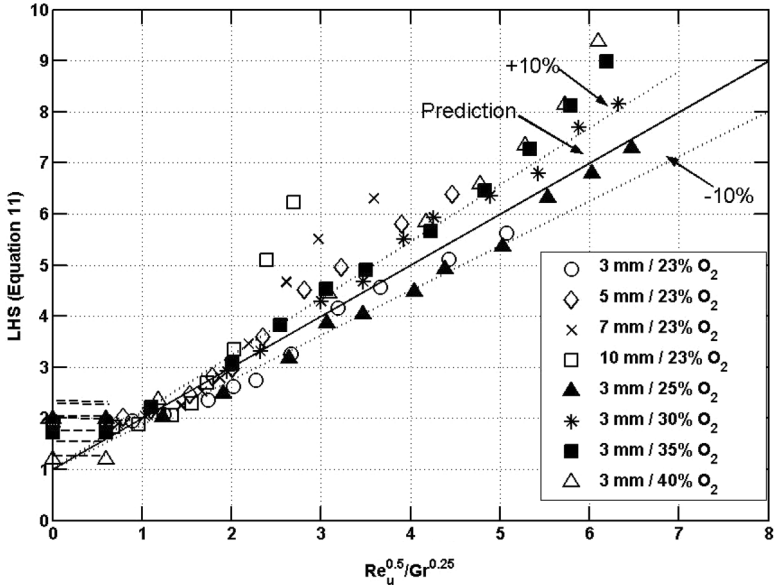

Figure 11. The plot of the left hand side of Equation (11) with $\mathrm{Re}_u^{0.5}/Gr^{0.25}$ for forward smolder. Note the wider uncertainty band at $\mathrm{Re}_u = 0$.

Figure 12 shows the plot of the *LHS* with $\mathrm{Re}_u^{0.5}/Gr^{0.25}$ for reverse smolder. The scatter in the data on this plot is smaller than in the original form (Figure 3), an indication that the correlation has captured the essential features of the behavior of smolder.

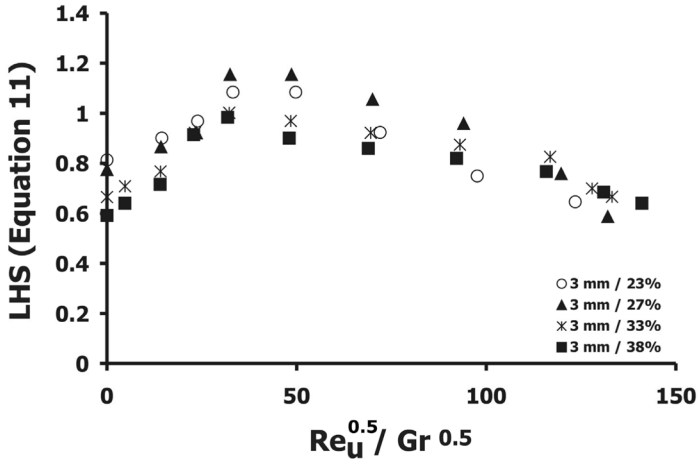

Figure 12. The plot of the left hand side of Equation (11) with $\mathrm{Re}_u^{0.5}/Gr^{0.25}$ for reverse smolder. Note the wider uncertainty band at $\mathrm{Re}_u = 0$.

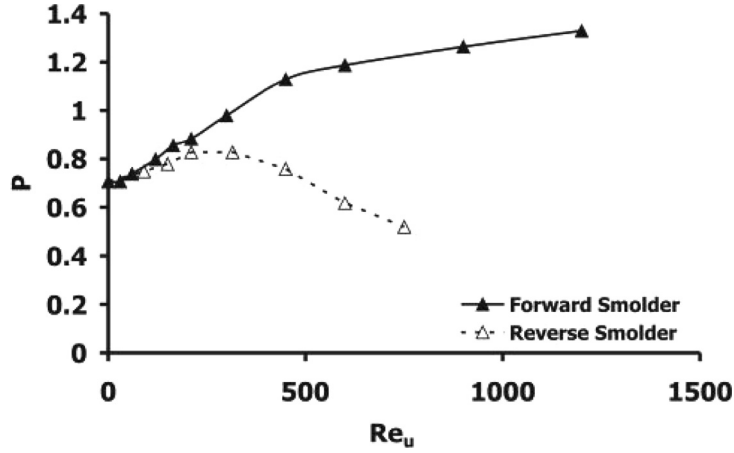

Figure 13. The variation of P with Re_u.

To understand the role played by radiation, we define a parameter P as the ratio of radiative heat flux to the heat flux that goes into propagating the smolder front.

$$P = \mathrm{Re}_r \Big/ \left[\frac{\varepsilon\sigma(T_s^4 - T_0^4)}{[\mu c_p/d_0](T_s - T_0)}\right] \tag{15}$$

The variation of P with the flow Reynolds number is plotted in Figure 13 for forward smolder. It is clear that the radiation term plays a significant role in the heat balance. In the case of forward smolder, it is about the same magnitude as the heat flux for propagation at lower stream velocities, and constitutes 70% of the heat flux for propagation at higher velocities. In the case of reverse smolder, the oxidizer flux from the gas phase decreases with the free stream speed leading to reduced heat generation rate at the surface. This makes the radiant heat loss far more significant and leads to the reduction in smolder rate beyond some stream speed ultimately leading to extinction. This feature is similar to that noticed by Olsen and T'ien (2000).

CONCLUDING REMARKS

This article has dealt with the smoldering combustion of incense sticks. Experimental data on the effect of the velocity of the stream and its oxidiser mass fraction as well as the size of the sticks on the smoldering rate have been obtained and these have been explained on the basis of an energy balance. While forward smolder rates increase with stream speed, those for reverse smolder have a peak in the smolder rate. The reduction

in smolder rate with speed is due to *reduced* mass transport of the oxidizer from the recirculation zone associated with the reverse smolder process. One of the interesting results of this work that needed the use of computational fluid dynamics is the behavior of the back wall heat transfer with free stream flow, a feature not addressed usually because it has been found not very important, otherwise.

REFERENCES

Blasi, C.D. (1993) Modeling and simulation of combustion processes of charring and non-charring solid fuels. *Progr. Ener. Combus. Sci.*, **19**, 71–104.

Esfahani. (2002) Oxygen-sensitive thermal degradation of PMMA: A numerical study. *Combus. Sci. and Technol.*, **174**, 183–198.

Isachenko, V.P., Osipova, V.A., and Sukomel, A.S. (1977) Heat Transfer, Mir Publishers, Moscow.

Kashiwagi, T. (1994) Polymer Combustion and Flammability–Role of the Condensed Phase, 25th Symposium (International) on Combustion, The Combustion Institute, Pittsburgh, PA, pp. 1423–1437.

Kashiwagi, T. and Ohlemiller, T.J. (1982) A Study of Oxygen Effects on Nonflaming Transient Gasification of PMMA and PE During Irradiation, 19th Symposium (International) on Combustion, The Combustion Institute, Pittsburgh, PA, pp. 815–823.

Kutataladze, S.S. and Leontev, A.I. (1964) Turbulent Boundary Layers in Compressible Gases, Translated by D. B. Spalding, Academic Press, New York.

Ohlemiller, T.J. (1985) Modelling of smoldering combustion propagation. *Progr. Energy and Combustion Science*, **11**, 277–310.

Ohlemiller, T.J. (1995) Smoldering Combustion, SEPE Handbook of Fire Protection Engineering, 2nd Ed., Section 2, Chapter 11, National Fire Protection Assoc., Quincy, M.A., DiNenno, P.J., Beyler, C.L., Custer, R.L.P., Walton, W.D., Eds., **2**, 171–179.

Olsen, S.L. and T'ien, J.S. (2000) Buoyant low stretch diffusion flames beneath cylindrical PMMA samples. *Combust. Flame*, **121**, 439–452.

Paul, P.J., Mukunda, H.S., and Jain, V.K. (1982) Regression Rates in Boundary Layer Combustion, 19th Symposium (International) on Combustion, The Combustion Institute, pp. 717–729.

Williams, F.A. (1976) Mechanism of Fire Spread, Sixteenth Symposium (International) on Combustion, pp. 1281–1294.